



Source and variation of carbonaceous aerosols at Mount Tai, North China: Results from a semi-continuous instrument

Zhe Wang^a, Tao Wang^{a,b,c}, Rui Gao^a, Likun Xue^{a,b}, Jia Guo^b, Yang Zhou^a, Wei Nie^{a,b}, Xinfeng Wang^{a,b}, Pengju Xu^a, Jian Gao^{a,c}, Xuehua Zhou^a, Wenxing Wang^{a,c}, Qingzhu Zhang^{a,*}

^a Environment Research Institute, Shandong University, Shanda Nanlu 27, Ji'nan, Shandong 250100, PR China

^b Department of Civil and Structural Engineering, The Hong Kong Polytechnic University, Hong Kong, PR China

^c Chinese Research Academy of Environmental Sciences, Beijing 100012, PR China

ARTICLE INFO

Article history:

Received 10 October 2010

Received in revised form

30 December 2010

Accepted 3 November 2011

Keywords:

Carbonaceous aerosols

Semi-volatile organic carbon (SVOC)

Secondary organic aerosol (SOA)

Source analysis

Mount Tai (Mt. Tai)

ABSTRACT

Carbonaceous aerosols were measured with a semi-continuous thermal-optical OC/EC analyzer at the summit of Mount Tai (1532.7 m a.s.l) in north China during spring and summer of 2007. Non-volatile organic carbon (NVOC) and elemental carbon (EC) showed high concentrations with mean values of 6.07, 1.77 and 5.05, 0.99 $\mu\text{g m}^{-3}$ in spring and summer, respectively. The mean concentration of semi-volatile organic carbon (SVOC) was 6.26 $\mu\text{g m}^{-3}$ in spring and 13.33 $\mu\text{g m}^{-3}$ in summer, contributing 51 and 72% to total organic carbon (TOC), respectively. Different measurement methods for EC were compared, and a good agreement between optical and thermal methods was found. Due to volatilization of SVOC during sampling, the integrated filter measurement without denuder and backup absorbent tended to underestimate TOC compared to semi-continuous measurement. Principal component analysis (PCA) and hierarchical cluster analysis (HCA) results indicated that the observed carbonaceous aerosols at Mount Tai were mostly contributed by the transport of aged aerosols in the planetary boundary layer (PBL) mixed with combined sources. Also, the influence of emissions from Korea was observed at Mount Tai, as well as biomass burning. Cloud processing contributed to elevated SVOC concentrations, and the formation of secondary organic aerosol (SOA) through photochemistry and cloud processing were both enhanced in summer. Clean air masses from the free troposphere reduced carbonaceous concentrations, and the regional background condition with $2.13 \pm 1.05 \mu\text{g m}^{-3}$ of NVOC, $0.43 \pm 0.29 \mu\text{g m}^{-3}$ of EC, and 2.40 to 6.80 $\mu\text{g m}^{-3}$ of SVOC (for spring and summer, respectively) were suggested for the North China Plain.

© 2011 Elsevier Ltd. All rights reserved.

1. Introduction

Atmospheric carbonaceous aerosols are major components of fine particles (Seinfeld and Pandis, 1998), and are usually classified into three main fractions: organic carbon (OC), elemental carbon (EC), and inorganic carbon (mainly crustal carbonate). The major source of EC is incomplete combustion of fossil fuels and biomass materials, whereas OC could be directly emitted from primary anthropogenic and biogenic sources or produced by secondary formation via the gas-to-particle conversion process (Seinfeld and Pandis, 1998). Carbonaceous aerosols have significant impacts on the climate and human health (Jacobson, 2001; Menon et al., 2002; Sun and Ariya,

2006); to understand these effects, the physical-chemical properties of carbonaceous aerosols have been extensively studied.

A majority of previous investigations of atmospheric carbonaceous aerosols were based on integrated filter collection with off-line laboratory analysis, and some measured black carbon (BC) or EC in real-time using optical attenuation method (Husain et al., 2007; Kanaya et al., 2008), and some also employed an in-situ semi-continuous OC/EC analyzer (Plaza et al., 2006; Saarikoski et al., 2008). Both positive artifacts caused by adsorption of gaseous organics and negative artifact from evaporation of collected OC have been found in integrated measurements (Lim et al., 2003; Cheng et al., 2009, 2010). Significant differences in EC measurement have been reported between optical and thermal methods (Jeong et al., 2004; Park et al., 2006; Bae et al., 2007; Husain et al., 2007; Kanaya et al., 2008), and the different results were found on the comparison because of the different sources and physical-chemical properties of aerosols in different areas. Therefore, there is a need

* Corresponding author. Tel.: +86 531 88364435; fax: +86 531 88369788.

E-mail address: zqz@sdu.edu.cn (Q. Zhang).

for the continuing assessment and systematical comparison between these methods under various environmental conditions.

Increased usages of fossil fuels as well as biomass burning in China are thought to have a significant impact on carbonaceous aerosols on regional scales. Many studies conducted in urban areas in China have reported high carbonaceous concentrations from coal combustion and traffic exhausts, with a contribution of 25–80% to fine particles (Dan et al., 2004; Cao et al., 2007; Meng et al., 2007). Measurements of carbonaceous aerosols in rural background and high-altitude sites with regional representativeness have started to emerge in recent years (Chow et al., 2006; Gelencser et al., 2007; Rengarajan et al., 2007; Ram et al., 2008), however, there are only limited studies on rural and mountain sites in China (Han et al., 2008; Zhang et al., 2008; Cao et al., 2009). Most of the earlier studies in China and overseas on organic carbon were mainly on the non-volatile fraction as they did not include the semi-volatile part, which was easily lost during sampling, but could account for 10–70% of the organic carbon (Cheng et al., 2009).

The North China Plain is one of the most developed regions of China, and is among the areas with the greatest emissions of anthropogenic aerosols in the country (Zhang et al., 2009). Remarkable carbonaceous pollutions have been reported in big cities in this region (e.g., Beijing, Tianjin and Zhengzhou) (Dan et al., 2004; Cao et al., 2007; Zhang et al., 2008). Mount Tai (Mt. Tai) is the highest mountain in this area, and atmospheric data collected on the summit can provide valuable information on sources and atmospheric processing of air pollutions in the North China plain. Therefore, it has attracted a lot of attention from researchers for studying gaseous, aerosols and rain chemistry (Gao et al., 2005; Fu et al., 2008; Kanaya et al., 2008; Ren et al., 2009; Zhou et al., 2010).

As part of an extensive study of a China's National Basic Research Project, two intensive measurement campaigns were conducted on aerosols, trace gases, cloud and rain waters at Mt. Tai in spring and summer of 2007. A dual oven semi-continuous OC/EC analyzer, which was initially developed and tested in 2005 (Grover et al., 2009), was employed in the present study and simultaneously measured semi-volatile organic carbon (SVOC), non-volatile organic carbon (NVOC) and EC, addressing the needs expressed above. In this paper, we report the concentrations and temporal variations of different carbonaceous species, examine the performance of different measurement methods, and investigate the sources and processes that affect the variation of the carbonaceous aerosols.

2. Experimental

2.1. Measurement site

The measurement site was located in a meteorological observatory on the summit of Mt. Tai (36.25 N, 117.10E, 1532.7 m asl) in Shandong Province of China. The city of Tai'an (population: 0.5 million) is 15 km south and the city of Jinan (capital of Shandong Province with population of 2.1 million) is 60 km north of the site. There are many tourists on the mountain in the summer months (June–September), and consequently some local emissions emitted from small restaurants and temples (Gao et al., 2005). The measurement site was situated on the less frequently visited eastern part of the summit, which is rarely disturbed by tourism and local sources (Gao et al., 2005; Ren et al., 2009). The experiments were performed from March 22 to April 24 for the spring campaign and from June 16 to July 20 for the summer campaign. During campaigns, the daily temperature varied between -3 to 13 °C in spring and 13 to 22 °C in summer; mean RH ranged between 25 to 98% in spring and 24 to 100% in summer; winds were relatively larger (4 to 15 m s^{-1}) in spring than summer (2 to 9 m s^{-1}), and generally remained southerly/southwesterly in spring and more easterly in summer.

2.2. Dual-oven semi-continuous OC/EC aerosol analyzer

Time-resolved carbonaceous aerosols were measured by a semi-continuous OC/EC analyzer (Dual-oven model, Sunset Laboratory Inc.), and a schematic layout of the instrument is shown in Fig. 1. Different from the single-oven analyzers used in previous studies (Kanaya et al., 2008; Saarikoski et al., 2008), the dual-oven analyzer had a second quartz oven, which contained a carbon-impregnated filter (CIF) and was mounted in-line with the first oven. The sampled air passed through a parallel-plate organic denuder (Sunset Laboratory Inc.) to remove gaseous organic compound with an expected efficiency of better than 99% (Grover et al., 2009), and the aerosols were collected by a quartz filter in first oven, and then analyzed as NVOC. The particle-free air then continued to the second oven, in which any evaporated semi-volatile organic compounds during sampling were collected by the CIF, which was defined as SVOC. After the collection, different stepwise heating programs were performed in the two ovens to thermally desorb

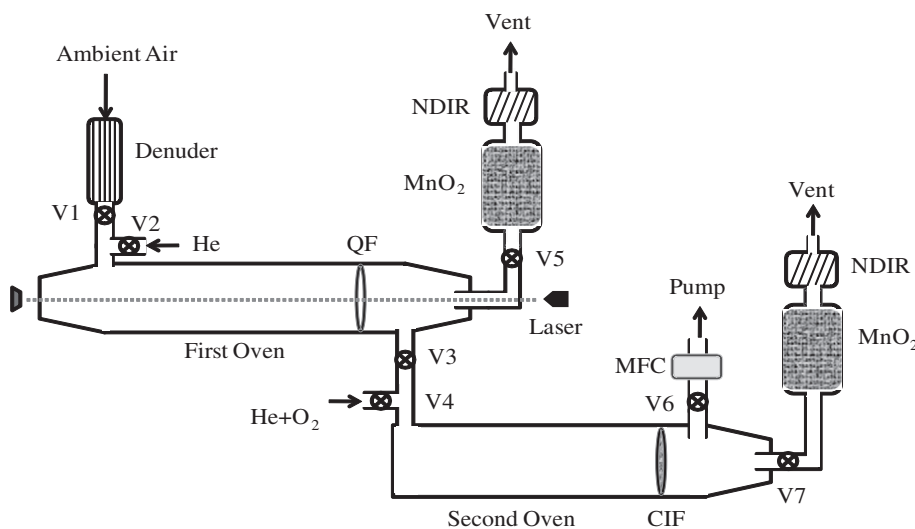


Fig. 1. Schematic layout of the dual-oven semi-continuous OC/EC aerosol analyzer. Key: V#, electrical valve; QF, quartz filter; MnO₂, MnO₂ oxidizing oven; NDIR, non-dispersive infrared detectors; MFC, mass flow control; CIF, carbon-impregnated filter. During sampling-mode, valve 1, 3 and 6 are open, and others remain closed; for analyzing-mode, valve 1, 3 and 6 is closed, and valve 2, 4, 5 and 7 are open.

Table 1

Summary of measured concentrations ($\mu\text{g m}^{-3}$) of different carbonaceous fractions in $\text{PM}_{2.5}$ at the summit of Mt. Tai in spring and summer of 2007.

	Spring (N ^a = 574)				Summer (N = 792)			
	Mean	SD	Min	Max	Mean	SD	Min	Max
NVOC	6.07	2.97	BDL ^b	18.10	5.05	2.62	BDL	15.70
NVOC1	1.99	0.92	0.17	6.32	1.57	0.77	BDL	4.25
NVOC2	1.59	0.86	BDL	5.45	1.28	0.74	BDL	6.34
NVOC3	1.55	1.22	BDL	6.81	1.38	0.98	BDL	5.25
PC	0.94	0.80	BDL	4.81	0.82	0.58	BDL	3.63
EC	1.77	1.59	BDL	13.92	0.99	0.68	BDL	3.56
SVOC	6.26	4.87	0.79	37.53	13.33	8.62	0.19	48.45
SVOC1	3.51	2.90	0.40	22.44	5.16	3.68	BDL	20.55
SVOC2	2.75	2.26	BDL	17.37	8.17	5.23	BDL	28.25
TOC	12.33	6.20	2.14	46.07	18.39	9.68	0.23	55.74
TC	14.1	6.97	2.17	47.11	19.37	9.94	0.58	56.15
NVOC/EC	5.0	3.7	0.5	35.5	6.2	3.8	0.8	33.9
SVOC/NVOC	1.4	2.4	0.2	41.5	3.3	3.5	0.1	36.6

^a Number of data samples.

^b BDL: below detection limit.

and pyrolyze the collected species into a MnO_2 oxidizing oven, and then the converted CO_2 was quantified by non-dispersive infrared (NDIR) detectors.

For the first oven, two-stage thermal analysis (250–450–620 °C in He atmosphere and 500–700–830 °C in an oxidizing atmosphere (98% He + 2% O_2)) was employed to analyze the non-volatile carbonaceous species. In order to minimize the influence of catalytic metal oxidation (Harrison and Yin, 2008), the highest temperature in the He mode was slightly adjusted and lower than the NIOSH method (Birch and Cary, 1996; NIOSH, 1996) but higher than the IMPROVE protocol (Chow et al., 2001; Kanaya et al., 2008). The OC/EC split was determined by the thermal-optical transmittance (TOT) method (Birch and Cary, 1996). The analysis of SVOC in the second oven was conducted in an oxidizing atmosphere (98% He + 2% O_2), operating with a two-steps heating program (170–310 °C). The maximum temperature for analyzing this fraction was far too low to oxidize any of the EC off the filter, but hot enough to vaporize nearly all of collected organic compounds on CIF. This method produced four NVOC fractions

(NVOC1, NVOC2, NVOC3 and PC (pyrolyzed carbon)), three EC fractions (EC1, EC2 and EC3) and two SVOC fractions (SVOC1 and SVOC2). In addition, this instrument also provided real-time optical EC data by detecting the change of a laser beam (660 nm) passing through the mounted filter in the first oven during sampling.

The sampling inlet was equipped with a $\text{PM}_{2.5}$ cyclone, with a flow rate of 8 L min^{-1} . An hourly measurement cycle was used with 45-minutes sampling and 15-minutes analysis. At the end of each analysis, a fixed volume loop of methane (5% methane in He) was automatically injected as an internal standard to normalize the results and minimize the variation of instrument performance. Multipoint sucrose standard calibrations were conducted at the start and the end of campaigns. Single-point sucrose standard and gas syringe standard validations were performed periodically during the campaigns. The reported carbonaceous concentrations were derived by subtracting the instrumental blanks, which was carried out at 0:00 every day. Very small amount of data clearly recognized as influence of burning plume from temples has been discarded as “noise” data. The detection limit for NVOC, SVOC and EC based on the thermal method was $0.3 \mu\text{g cm}^{-3}$, but was $0.13 \mu\text{g cm}^{-3}$ for EC with the optical method.

2.3. Integrated filter measurement and Aethalometer

The 24-h $\text{PM}_{2.5}$ samples were collected on quartz filters (Pallflex #2500 QAT-UP, Pall Gelman Inc.) placed in a Thermo Andersen Chemical Speciation Monitor (Thermo Electron Corporation, RAAS2.5-400). All the quartz filters were pre-heated at 600 °C and the collected samples were stored in a freezer at $-4 \text{ }^\circ\text{C}$ prior to analysis. A portion of the filter (2.3 cm^2) was punched from the $\text{PM}_{2.5}$ quartz filter for carbonaceous analysis by the same OC/EC analyzer as described above, operating in off-line mode. The analytical procedure employed here was 250–450–650–830 °C in a He atmosphere and 600–700–830 °C in an oxidizing atmosphere. The detection limit was $0.04 \mu\text{g m}^{-3}$ for 24-h filter samples.

An Aethalometer (Magee Scientific Model AE21) was employed during the spring campaign to continuously measure

Table 2

Comparison of measured OC and EC concentrations and OC/EC ratios among different high-altitude sites and rural background sites in the world.

Location	Elevation (km)	Sampling Period	Size	OC ($\mu\text{g m}^{-3}$)	EC ($\mu\text{g m}^{-3}$)	OC/EC	Reference
Manora Peak, India	1.95	Feb–Mar 2005	TSP	11.6	1.8	6.6	Ram et al., 2008
		Apr–Jun 2005	TSP	8.6	0.9	11	
		Dec–Mar 2006	TSP	11	1.5	8.2	
Mt. Abu, India	1.7	Dec–Mar 2005	TSP	3.6	0.8	4.8	Ram et al., 2008
Manora Peak, India	1.95	Dec 2004	TSP	4.8	0.81		Rengarajan et al., 2007
Nylsrlley, South Africa	1.1	May 1997	TSP	14.1	0.85		Puxbaum et al., 2000
Muztagh Ata Mountain, China	4.5	Spring	TSP	0.36	0.038		Cao et al., 2009
		Summer	TSP	0.77	0.071		
Nagarkot, Nepal	2.15	Feb–May 2000	PM_{10}	14.375	0.94		Carrico et al., 2003
Langtang, Nepal	3.92	Feb–May 2000	PM_{10}	3.44	0.3		Carrico et al., 2003
Mt. Sonnblick, Austria	3.1	July 1996	PM_{10}	53.7	5.0		Hitzenberger et al., 1999
Dunhuang, China	1.139	2006	PM_{10}	16.2	3.8		Zhang et al., 2008
		2006	PM_{10}	29.3	4.1	8.7	
Shangri-La, China	3.583	2006	PM_{10}	3.1	0.34	11.9	Zhang et al., 2008
Zhenbeitai, China	1.135	2006	PM_{10}	11.9	4	4.2	Zhang et al., 2008
Stara Lesna, Slovakia	0.808	2002–2003	PM_{10}	4.32	0.8		Yttri et al., 2007
Braganza, Portugal	0.690	2002–2003	PM_{10}	4.1	0.79		Yttri et al., 2007
Daihai, China	1.221	Apr–May 2007	$\text{PM}_{2.5}$	8.1	1.81	5	Han et al., 2008
		Jun–Jul 2006	$\text{PM}_{2.5}$	8.7	1.4	6.2	
Puy de Dome, central France	1.450	Jun–Jul, 2003	$\text{PM}_{2.5}$	4.63	0.29		Gelencser et al., 2007
Schauinsland, Germany	1.205	Jun–Aug, 2003	$\text{PM}_{2.5}$	3.8	0.25		Gelencser et al., 2007
Sonnblick, Austrian Alps	3.106	May–Jun 2003	$\text{PM}_{2.5}$	1.44	0.12		Gelencser et al., 2007
Olancha, California	1.124	Dec 1999–Feb 2001	$\text{PM}_{2.5}$	2.86	0.7		Chow et al., 2006
Mojave-Poole, California	0.832	Dec 1999–Feb 2001	$\text{PM}_{2.5}$	3.57	1.1		Chow et al., 2006
Mt. Tai, China	1.533	Mar–Apr 2007	$\text{PM}_{2.5}$	6.07 ^a	1.77	5.0	This study ^a
Mt. Tai, China	1.533	Jun–Jul 2007	$\text{PM}_{2.5}$	5.05 ^a	0.99	6.2	This study

^a Considering that most of the previously literature data are obtained using the method for non-volatile aerosol, only NVOC is compared.

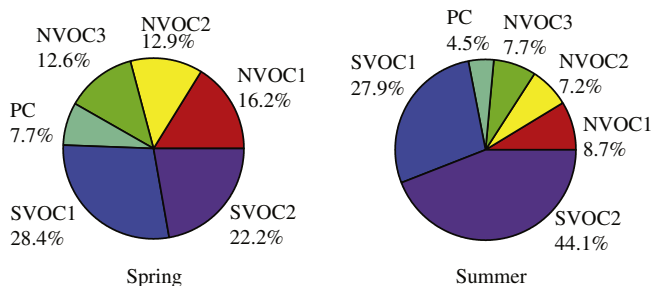


Fig. 2. Contribution of different OC fractions to TOC in $PM_{2.5}$ during spring and summer campaigns in 2007 at Mt. Tai, China.

BC in $PM_{2.5}$. A detailed description of this instrument was given by Zhou et al. (2009). In this study, 2 wavelengths (880 and 370 nm) were employed, corresponding to BC and UV-absorbing Particulate Material (UVPM, which can represent the “blue” material that absorbed UV photons with the same efficiency as BC does). Mass absorption cross sections of 16.6 and $39.5 \text{ m}^2 \text{ g}^{-1}$ were used as recommended by the manufacturer to convert the observed light attenuation to mass concentration of BC and UVPM, respectively.

3. Results and discussion

3.1. Abundances of carbonaceous content in $PM_{2.5}$

3.1.1. Concentrations of NVOC, SVOC and EC

A statistical summary of carbonaceous concentrations measured in both campaigns at Mt. Tai is presented in Table 1. NVOC and EC show higher concentrations in spring (6.07 and $1.77 \mu\text{g m}^{-3}$) than in summer (5.05 and $0.99 \mu\text{g m}^{-3}$), suggesting the impact of coal combustion by heating in early spring and efficient wash-out by rain and cloud in summer. The observed concentrations of NVOC and EC in $PM_{2.5}$ at Mt. Tai were apparently higher compared to background or mountain sites in Europe and America, and were comparable to or even higher than coarse carbonaceous concentrations at mountain sites in Asia, as summarized in Table 2.

SVOC exhibits higher concentrations than NVOC in both seasons (Table 1), with average SVOC/NVOC ratio of 1.4 in spring and 3.3 in summer. By taking SVOC into account, the concentrations of total organic carbon (TOC) are 12.33 and $18.39 \mu\text{g m}^{-3}$ in spring and summer, respectively. Previous studies based on integrated filter method have reported that the ratio of organic matters (OM) to OC varied from 1.2 to 2.2, due to different sources and properties of aerosols (Chan et al., 2010). However, little information can be found on the conversion ratio of SVOC. Considering the relatively

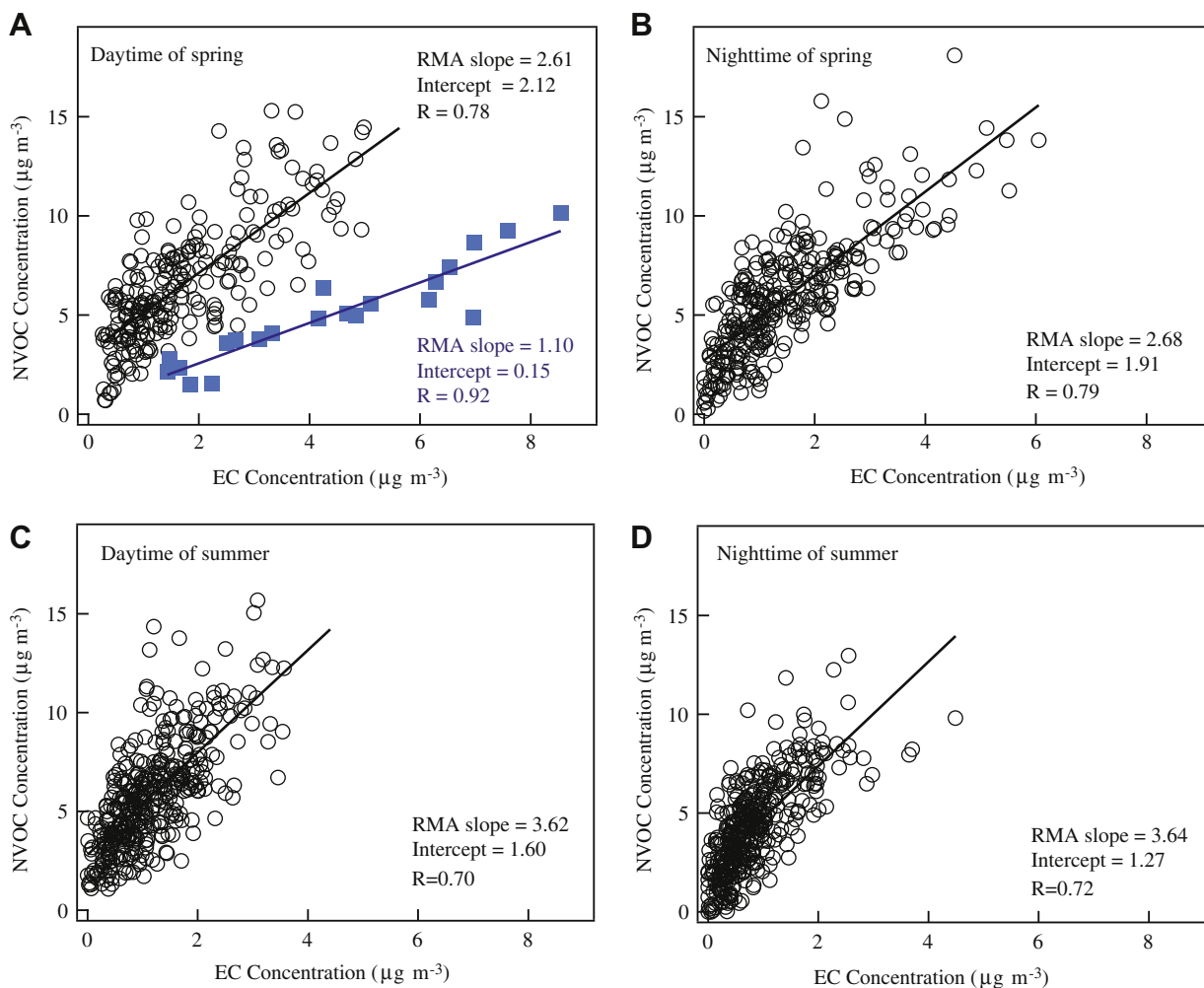


Fig. 3. Scatter plots of NVOC and EC concentrations in $PM_{2.5}$ at Mt. Tai during (A) daytime and (B) nighttime in spring and (C) daytime and (D) nighttime in summer. The black circles represent non-episodic data and full squares in panel A represent the episodes that occurred on April 15, 18, 19 and April 21. The solid lines show the linear fits.

low volatility of SVOC and high-altitude site condition, conversion ratios of 1.4 for SVOC and 1.8 for NVOC were used in the present study, and the resulting OM accounted for 52% and 66% of $PM_{2.5}$ mass in spring and summer, respectively.

Different OC fractions were separated by stepwise heating program based on their volatility and thermal stability, and their contributions to TOC are presented in Fig. 2. As shown, the concentrations of different fractions decrease as the molecular weight increases, except the enhanced SVOC2 in summer. SVOC accounts for 51% and 72% of TOC in spring and summer, respectively, indicating the predominant contribution of semi-volatile species to the organic particulate loading in this region. Notable increase of SVOC in summer may suggest enhanced SOA formation, and also was linked to the high temperature in summer that would favor the volatilization of collected organic aerosols in first oven, and result in more SVOC collected in the backup oven. NVOC1 corresponds to lower molecular weight with volatilization at $T < 250$ °C, having similar contribution to NVOC in both seasons. Higher molecular weight fractions (NVOC2, NVOC3, PC) as more aged and oxygenated species, exhibit lower concentrations in the night, which can be explained by the weak emission sources and the absence of the photochemical aging process during the night.

3.1.2. Relationship between NVOC and EC

The relationship between OC and EC can provide some indication of the origin of carbonaceous aerosols, chemical process and removal effect (Han et al., 2008; Cao et al., 2009). The mean NVOC/EC ratios are 5.0 in spring and 6.2 in summer, with slightly lower values in daytime than nighttime. These ratios are comparable to those measured at other regional and mountain sites in the world (4.2–12) (cf. Table 2). Including SVOC, the TOC/EC ratios increase to 10.9 in spring and 20.4 in summer. Aging of air masses leads to a high OC/EC ratio due to the SOA formation through oxidation and condensation of organic materials. The observed high OC/EC ratios here suggest the dominant aged aerosols from long-range transport. Coal combustion and biomass burning have also been

reported to yield high NVOC/EC ratios (Meng et al., 2007; Han et al., 2008).

Good correlations between NVOC and EC in both seasons are depicted in Fig. 3. The products of RMA slope and EC are usually related to OC from combustion sources (e.g., fossil fuels), while the intercepts are related to the OC from non-combustion sources. Seasonal variations are clearly shown for both combustion (i.e., slopes) and non-combustion sources (i.e., intercepts). In each season, the combustion sources for OC are relatively stable but the non-combustion sources are reduced in nighttime. Air masses with high NO_x concentrations and low NVOC/EC ratios were observed in daytime of April 15, 18, 19 and 21, giving a NVOC/EC RMA slope of 1.10 and an intercept of $0.15 \mu\text{g m}^{-3}$ (Fig. 3A). OC/EC ratios of 0.84 to 1.1 have been reported for vehicle exhaust (Watson et al., 2001; Plaza et al., 2006), and thus air masses observed on these days at Mt. Tai are apparently related to the transport of fresh traffic exhaust plumes from the urban area.

3.1.3. Diurnal variation

The diurnal evolutions of carbonaceous species are illustrated in Fig. 4. NVOC and EC exhibit a single-afternoon-peak at Mt. Tai in both seasons, similar to a suburban site impacted by the transport of urban plumes (Plaza et al., 2006). SVOC1 and SVOC2 show low broad peaks in spring afternoon, and the afternoon peaks are enhanced in summer. The elevated concentrations during afternoon are likely due to the upslope flow of pollution in the boundary-layer and enhanced daytime vertical convection (Ren et al., 2009). The diurnal variations are “noisier” in spring than in summer, which can be explained by stronger and more variable winds shifting the air mass from different regions in spring season.

In spring, EC reaches a local peak at 10:00 and decreases in concentration from 10:00 to 13:00, whereas NVOC reaches its first local maximum later than EC, which is similar to gas-phase peroxides and ozone (Ren et al., 2009), indicating the photochemical production of SOA. In summer, no significant delay is indicated for NVOC and EC, but 2 to 3 h delay after non-volatile

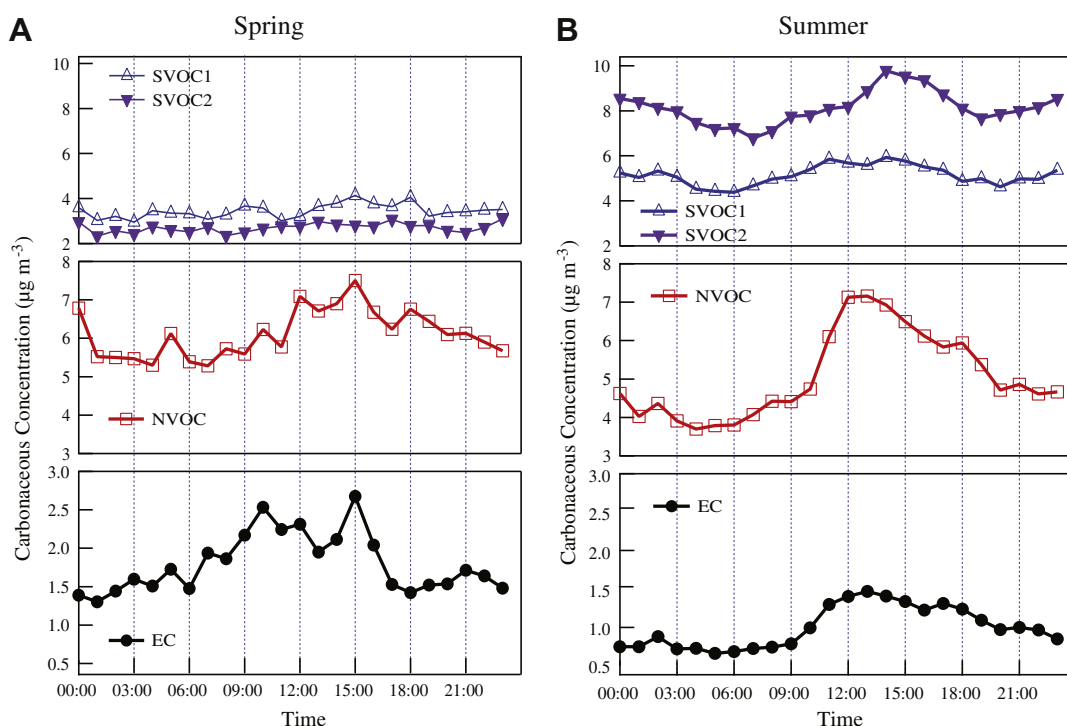


Fig. 4. Diurnal variations of SVOC, NVOC and EC concentrations during (A) the spring campaign and (B) the summer campaign at Mt. Tai.

species is found for SVOC, clearly indicating the SOA formation after the plumes with primary pollutions transported to the site. SVOC1 and SVOC2 both exhibit a local maximum during midnight, resulting in high semi-volatile ratio at night. Partitioning of low-volatility gas phase precursors to the particle phase at reduced temperature and enhanced RH has been reported (Morgan et al., 2010), and hence the low temperature and frequent cloud/fog events during nighttime at Mt. Tai both contribute to the significant abundance of SVOC. The enhanced SVOC concentration during cloud processes will be further discussed in later section (3.3).

3.2. Comparisons across different measurement methods

Fig. 5 illustrates the comparison among Thermal EC and Optical EC measured by Sunset OC/EC analyzer, BC and UVPM from Aethalometer. Excellent correlations ($R = 0.81$ – 0.98 , RMA slope = 0.70 – 1.18) are observed for all pairs, indicating general agreements among these methods. BC and UVPM exhibit the best

correlation ($R = 0.98$) with a RMA slope of 0.84 , similar to the mean ratio of 0.88 observed by Husain et al. (2007). UVPM and BC agree better at loading $< 8 \mu\text{g m}^{-3}$ (RMA slope = 0.93). Some data with a high UVPM/BC ratio at moderate loading indicate the existence of UV-absorbing organic compounds (e.g., PAHs) as 'blue' carbon, but BC is apparently higher than UVPM at loading $> 8 \mu\text{g m}^{-3}$ (cf. Fig. 5), suggesting the change of aerosol optical property in high loading condition and that absorption cross section should vary, either or both. Optical EC is prone to give lower values than UVPM and BC, with RMA slope of 0.82 and 0.70 , respectively, which is likely due to the different attenuation coefficients employed in two instruments.

Thermal EC and Optical EC from Sunset show good agreement in both seasons ($R = 0.91, 0.81$), with a RMA slope of 1.18 and 1.11 , respectively. The thermal program employed here is different from NIOSH and IMPROVE methods, and hence our results are between the values (slope of 0.97 and 1.42) from those two methods reported by Kanaya et al. (2008). Excellent agreement is found between Thermal EC and UVPM (RMA slope: 0.99), but a slightly

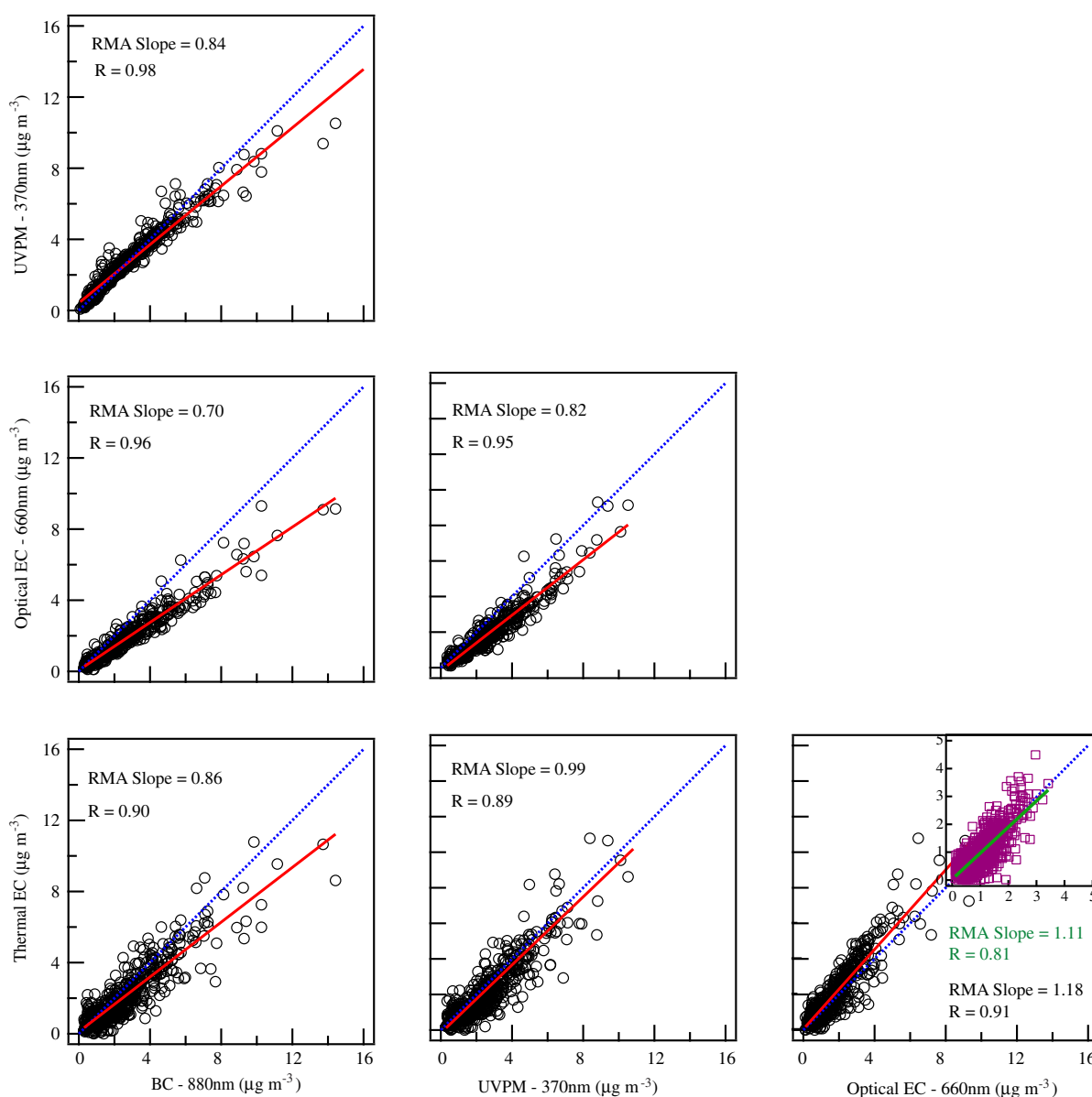


Fig. 5. Correlations for each pair among BC-880 nm (Aethalometer), UVPM-370 nm (Aethalometer), Optical EC-660 nm (Sunset) and Thermal EC (Sunset). Black circles represent data measured in the spring campaign, and the inset in the bottom right panel shows data measured in the summer campaign. Solid lines indicate the linear fit and blue dot lines represent the 1:1 lines (For interpretation of the references to color in this figure legend, the reader is referred to the web version of this article.).

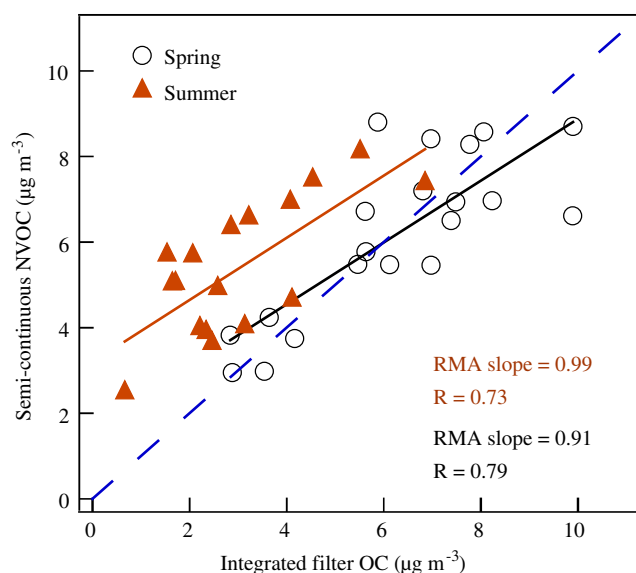


Fig. 6. Comparison scatter plots of semi-continuous and integrated filter measurements of NVOC. Black opened circles represent data measured in the spring campaign, and brown solid triangles represent the summer data. Solid and dot lines represents the linear fits, and blue dash line indicate the 1:1 line (For interpretation of the references to color in this figure legend, the reader is referred to the web version of this article.).

lower value is observed for Thermal EC than BC (RMA slope: 0.86). Husain et al. (2007) has reported 25% higher BC than Thermal EC, and a much higher discrepancy (2.7 to 3.3 times) was found by Jeong et al. (2004). In contrast, Bae et al. (2007) has observed higher Thermal EC than BC (slopes of 1.23–1.61). For Mt. Tai, the general relationship among these methods can be summarized as: Optical EC < Thermal EC ~ UVPM < BC. Considering EC from three optical methods straddle that from thermal method, we regard Thermal EC as more reliable in this study, and also because it is by a method that converts all materials to single-carbon compound (CO₂) and is quantitated with internal standard in every analysis.

Table 3
Component loadings from PCA of carbonaceous and related species in the spring campaign.

	Component 1	Component 2	Component 3	Component 4	Component 5
SVOC1			0.88	0.29	
SVOC2	0.20	0.15	0.71	0.30	
NVOC1	0.19	0.52	0.34	0.52	−0.12
NVOC2	0.30	0.87		0.23	
NVOC3	0.46	0.72		−0.18	−0.12
PC	0.34	0.71	0.12	−0.33	
EC	0.63	0.45	0.25	−0.28	−0.13
CO	0.74	0.35	0.21		0.25
NO	0.29	0.16	0.14	−0.75	−0.23
NOy	0.89	0.23	0.11		−0.18
O ₃	0.37	−0.12	0.34	0.66	0.13
SO ₂	0.81	0.27		−0.29	
Sulfate	0.83	0.22	0.21		
Ammonium	0.86	0.21	0.25	0.21	
Potassium	0.80	0.40	0.10		
Temperature		0.11		0.77	
RH	0.51		0.62	0.17	0.30
Solar		0.24	−0.12	0.61	0.28
<i>u</i>	0.14	0.19	0.57		−0.27
<i>v</i>	0.42	0.17	0.54		−0.66
Explained Variance	32.9%	17.3%	13.8%	9.8%	7.4%

n = 389, total explained variance 81.2%.

KMO test of sampling adequacy: 0.874 and Significance level of Bartlett's test: 0.

Loadings with absolute value less than 0.1 are not shown, and loadings greater than 0.5 are shown in bold.

u and *v* indicate the *x*- and *y*- (latitudinal and longitudinal) components of wind, positive values of *u* and *v* represents the west and south vector, respectively.

The daily integrated filter OC results and corresponding averaged semi-continuous NVOC concentrations are compared in Fig. 6. Good agreements between the two methods are shown, with RMA slope of 0.91 in spring and 0.99 in summer, similar to the results reported by Bae et al. (2004). The mean ratio of semi-continuous to integrated concentrations for NVOC in spring is 1.01, comparable to the ratio of 0.95–1.09 for OC reported by Lim et al. (2003). However, much higher ratios (i.e., 2.09) are found in summer at Mt. Tai. The difference is reflected in intercepts, rather than in slopes which are almost same in both seasons. The larger difference in summer can be explained by increased loss of collected OC on quartz filter during long time sampling at high temperature. Noting that only NVOC has been used in the comparison and if the SVOC was included, the ratio of semi-continuous TOC to filter based OC would increase to 1.91 in spring and 5.37 in summer. This suggests that almost half of TOC in spring and much higher amount in summer are not accounted for by the integrated filter-based measurement without denuder and backup absorbent. The EC from integrated and semi-continuous measurements showed significant difference (figure not shown), similar to the previously reported large discrepancy attributed to different analysis procedures, with the magnitude of difference from 21% to a factor of 2 (Chow et al., 2001; Kondo et al., 2006; Kanaya et al., 2008; Cheng et al., 2010).

3.3. Source analysis

In order to investigate the sources and factors that affect the variation of carbonaceous aerosols, principal component analysis (PCA) was employed (Fu et al., 2008; Ren et al., 2009). The different carbonaceous fractions, related gaseous and soluble inorganic species of PM_{2.5} were subjected to PCA with Varimax rotation. The measurement methods for these gases and aerosol components are given in Ren et al. (2009) and Zhou et al. (2010). The derived principal component loadings are presented in Table 3 and 4 for spring and summer, respectively.

3.3.1. PCA and case study in spring

In spring, five components were derived which explain 81.2% of the total variance. The first component has large contributions from

Table 4
Component loadings from PCA of carbonaceous and related species in the summer campaign.

	Component 1	Component 2	Component 3	Component 4	Component 5
SVOC1		0.26		0.81	0.11
SVOC2	0.19	0.30	0.14	0.82	
NVOC1	0.34	0.76	0.22		−0.35
NVOC2	0.27	0.87			−0.29
NVOC3	0.33	0.74	0.35	0.25	
PC	0.39	0.67	0.11		−0.15
EC	0.49	0.62	0.46	0.17	−0.10
CO	0.49		0.40	0.54	
NO _y	0.53	0.42	0.63		
O ₃	0.85	0.13	0.32		0.21
SO ₂	0.83	0.11	0.16		−0.13
Sulfate	0.58	0.22	0.69	0.11	
Ammonium	0.40	0.26	0.83	0.15	
Potassium	0.76	0.24	0.23		
Chloride	0.40	0.48	0.56	0.14	
Temperature		0.27	0.21	−0.51	0.58
RH		−0.17	0.50	0.76	0.55
Solar		0.22			
<i>u</i>			−0.13	−0.17	0.77
<i>v</i>	−0.19		0.22	−0.23	0.65
Explained variance	22.7%	20.3%	15.4%	14.5%	7.5%

$n = 522$, total explained variance 80.4%.

KMO test of sampling adequacy: 0.833 and Significance level of Barlett's test: 0.

Loadings with absolute value less than 0.1 are not shown, and loadings greater than 0.5 are shown in bold. *u* and *v* are the same as in Table 3.

EC, ammonium, sulfate, potassium, NO_y, SO₂ and CO, accounting for 32.9% of variances, and represents the transport of PBL pollution. Typical cases on April 6–7 is depicted in Fig. 7A, with 72-h back trajectory analysis from HYSPLIT 4 model (<http://www.arl.noaa.gov/ready/hysplit4.html>, NOAA Air Resources Laboratory) displayed in Fig. 7B. The simultaneous high concentrations of potassium, NO_y, SO₂ and CO indicate the combined sources for the transported aerosols, including biomass burning, traffic exhaust and coal combustion. The air masses passed over an area with intensive fire spots in north central China (NASA/University of Maryland, 2002) (Fig. 7B) which indicate the contribution of biomass burning to high NVOC and EC concentrations.

The second component shows high loadings for NVOC species, and is mainly associated with local anthropogenic sources contributing organic aerosols, explaining 17.3% of variance. Typical cases observed on April 10 and 21 (Fig. 7A) present significant increases of NVOC compared to other species. SVOC and RH exhibit high loadings in component 3, suggesting cloud processing, and the positive loading of *u* and *v* suggest the humid air transported from the southwest. The concentrations of NVOC and EC are decreased compared to the increase of SVOC during the cloud episodes on March 30 and April 11 (Fig. 7A). It suggests that the semi-volatile organic species are formed through aqueous phase reaction in cloud process. Increase of OC concentrations after fog episodes and highly correlated water soluble OC and water vapor have also been previously reported (Herckes et al., 2007; Hennigan et al., 2008). Further discussion of cloud effect on SVOC will be presented in subsequent work.

Large contributions of O₃, NVOC1, solar radiation and temperature, with positive loading of SVOC and negative loading of NO are observed in component 4, which is identified as SOA formation through photochemistry. It prevails in afternoon and a typical case on April 10 can be seen in Fig. 7A. Component 5 has high negative loadings from wind vector and negative loading from NVOC and gaseous species, representing the clean air mass from free troposphere. As shown for cases on April 22 and 23 (Fig. 7A), the concentrations of carbonaceous, gaseous and soluble species all display significant decrease. Back trajectory analysis (Fig. 7C) indicates that air masses originated from the north at high altitude, further supporting the clean air mass from the free troposphere.

3.3.2. PCA and case study in summer

For the summer campaign, five components are obtained and account for 80.4% of total variance (Table 4). Compared to one predominant component in spring, the first two components in summer contribute almost equally (i.e., 22.7% and 20.3% of variance). Component 1 shows high loadings from O₃, SO₂, NO_y, sulfate and potassium, with positive loadings of NVOC, EC and CO, which is associated with transport of chemically processed air mixed with biomass burning. Cases illustrating this component observed on June 17–18 are depicted in Fig. 8A, showing high concentrations of NVOC, EC and related species during this period. The more active photochemistry in summer favors the chemical processing of aerosols during transport, and the large peaks of potassium during cases indicate the strong influence of biomass burning (Zhou et al., 2010). This is further supported by back trajectory analysis coupled with fire spots (NASA/University of Maryland, 2002) in Fig. 8B, showing that the air masses travelled across Korea and east part of Shandong Province with intensive fire spots. The air masses transported at high altitude represent the regional condition above this area, suggesting that besides the sources in east China, emissions from Korea also probably contribute to the regional carbonaceous aerosol budget.

Large contributions of NVOC species and EC, with positive loadings from SVOC, NO_y and chloride are found in component 2, representing the transport of pollution in lower PBL. Fig. 8A depicts a typical case observed on June 19. NVOC species and EC exhibit high concentrations after midnight, while gaseous and soluble inorganic species exhibit low concentrations until a new air mass arrives and the cloud starts. Back trajectory analysis (Fig. 8C) indicates that air masses originated from Korea and travelled in lower PBL. The enhanced contribution of this component in summer suggests more influence from emissions in Korea, as well as local sources.

Component 3 shows high loadings from ammonium, sulfate, NO_y, chloride and RH, with positive loadings from NVOC and EC, and is identified as humid and aged air mixed with sea salt. A typical case on July 13 shows large peaks of NVOC, sulfate and chloride (Fig. 8A), and back trajectory (Fig. 8C) indicates that the air mass originated from northern part of China and travelled over the Bohai Sea. The high RH of this air mass provides favorable conditions for the formation of inorganic and organic aerosols through

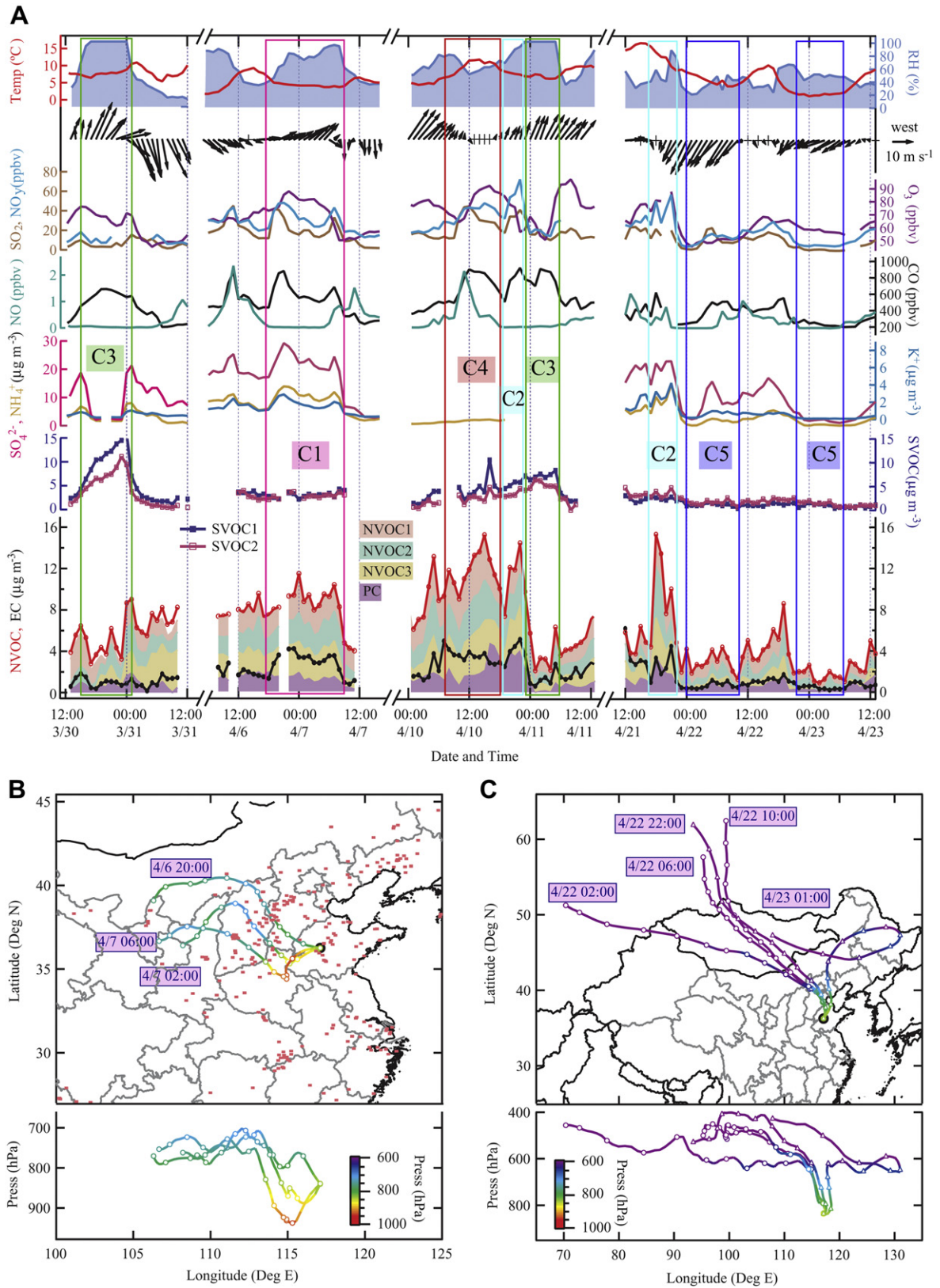


Fig. 7. (A) Time series of carbonaceous species, trace gases, soluble inorganic species and meteorological parameters for cases in spring of 2007. The colored rectangles indicate the typical cases discussed in the text, and C# represents the Component # from PCA in spring; Representative air mass back trajectories for (B) Component 1 on April 6–7 and (C) Component 5 on April 22–23 of 2007. Each back trajectory was calculated for 72 hours starting at 1500 m a.s.l, and the markers represent the location of the trajectories at a 6-h interval. The red solid squares in panel B represent the MODIS active fire spots for April 1–7 of 2007 (NASA/University of Maryland, 2002). (For interpretation of the references to color in this figure legend, the reader is referred to the web version of this article.)

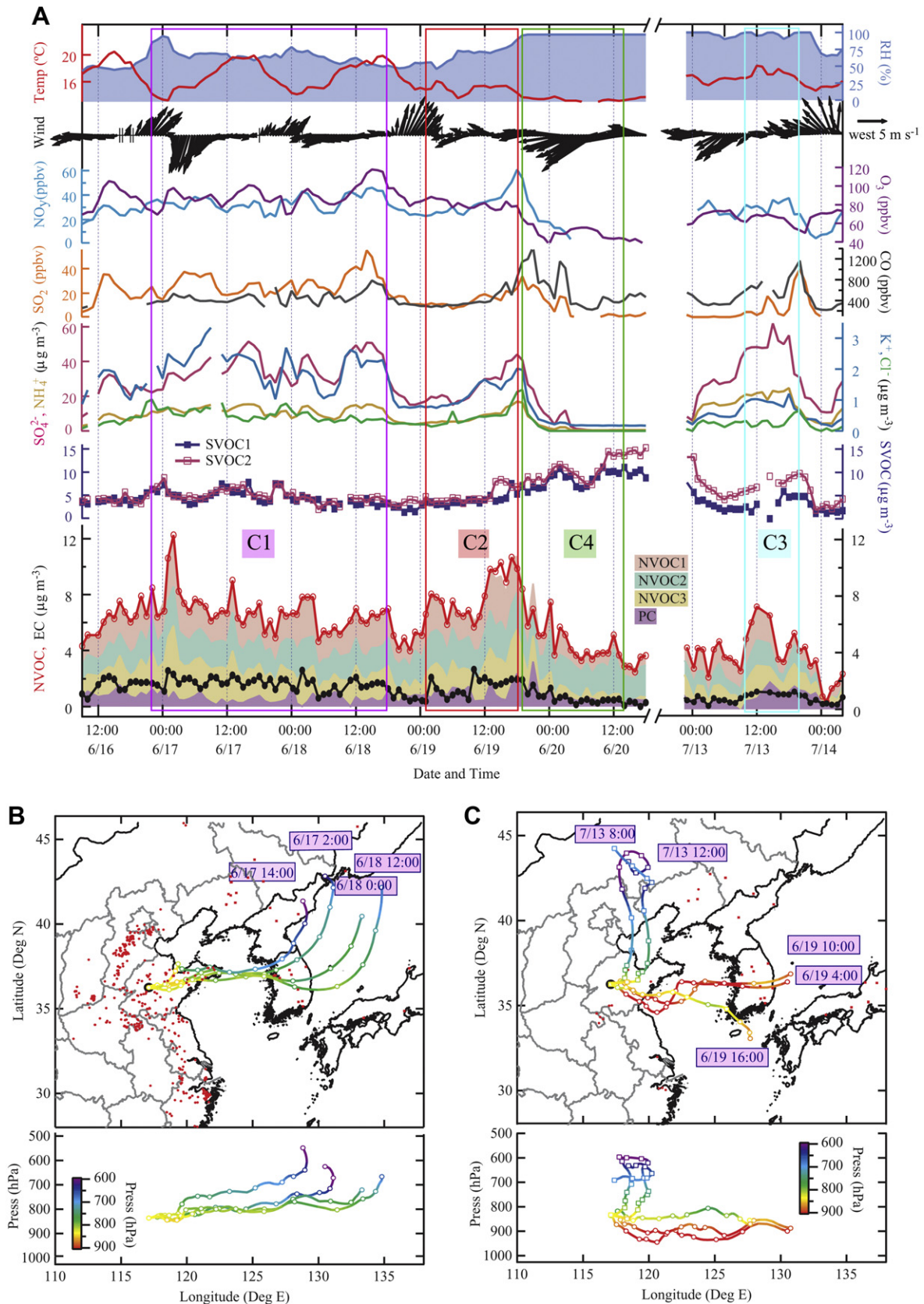


Fig. 8. (A) Time series of carbonaceous species, trace gases, soluble inorganic species and meteorological parameters for cases in summer of 2007. Notations are the same as in panel A of Fig. 7; (B) Representative air mass back trajectories for Component 2 on June 16–17 coupled with MODIS active fire spots. The red solid squares in Korea represent the fire spots for June 14–16, and the red dots in east China represent the fire spots for June 16–18; (C) Representative air mass back trajectories for Component 1 on June 19 and Component 3 on July 13, coupled with fire spots observed in Korea for June 16–17 and in east China for June 17–19. The back trajectories were obtained by use of the same approach described in Fig. 7. (For interpretation of the references to color in this figure legend, the reader is referred to the web version of this article.)

aqueous reaction. Component 4 has strong loadings of RH, SVOC and CO, with negative loading from temperature, representing cloud processing. A representative cloud case on June 20 is depicted in Fig. 8, and SVOC species increase compared to the decrease of other species, again suggesting the formation of SVOC through cloud processing. Component 5 has positive loading from wind vectors, temperature and solar radiation, indicating sunny and clear days with reduced carbonaceous concentrations. Likewise, this factor is related to clean air masses from the free troposphere and represents the background condition above this region.

3.3.3. Characterization of different origins

A hierarchical cluster analysis (HCA) was sequentially performed based on the principal component scores from PCA results. HCA was carried out by means of between-groups linkage, using squared Euclidean distances as a measure of similarity, and the results were represented by a dendrogram. Five well-separated groups dominated by each component are selected from the

hierarchy as the final, aggregated cluster solution. The statistic summary of carbonaceous concentrations for subgroups is presented in Fig. 9. As shown, the highest concentrations of NVOC and EC in spring are associated with transport of PBL pollution. In summer, the highest NVOC concentration is from the transport of pollutions in lower PBL, while chemically processed air mixed with biomass burning contributes the highest EC concentration. Photochemistry dominated the highest NVOC1 concentration in spring, indicating active SOA formation. The high concentrations of higher molecular weight fractions (NVOC3 and PC) from transport sources suggest more oxygenated and lower volatility species being formed through chemical process.

SVOC displays high concentrations from cloud processing in both seasons, and the concentration is almost doubled in summer, implying the increased SOA formation from both aqueous reaction and photochemistry. In contrast, NVOC and EC exhibit low concentrations in cloud processing due to efficient removal by cloud. The lowest concentrations of all carbonaceous species are found in the

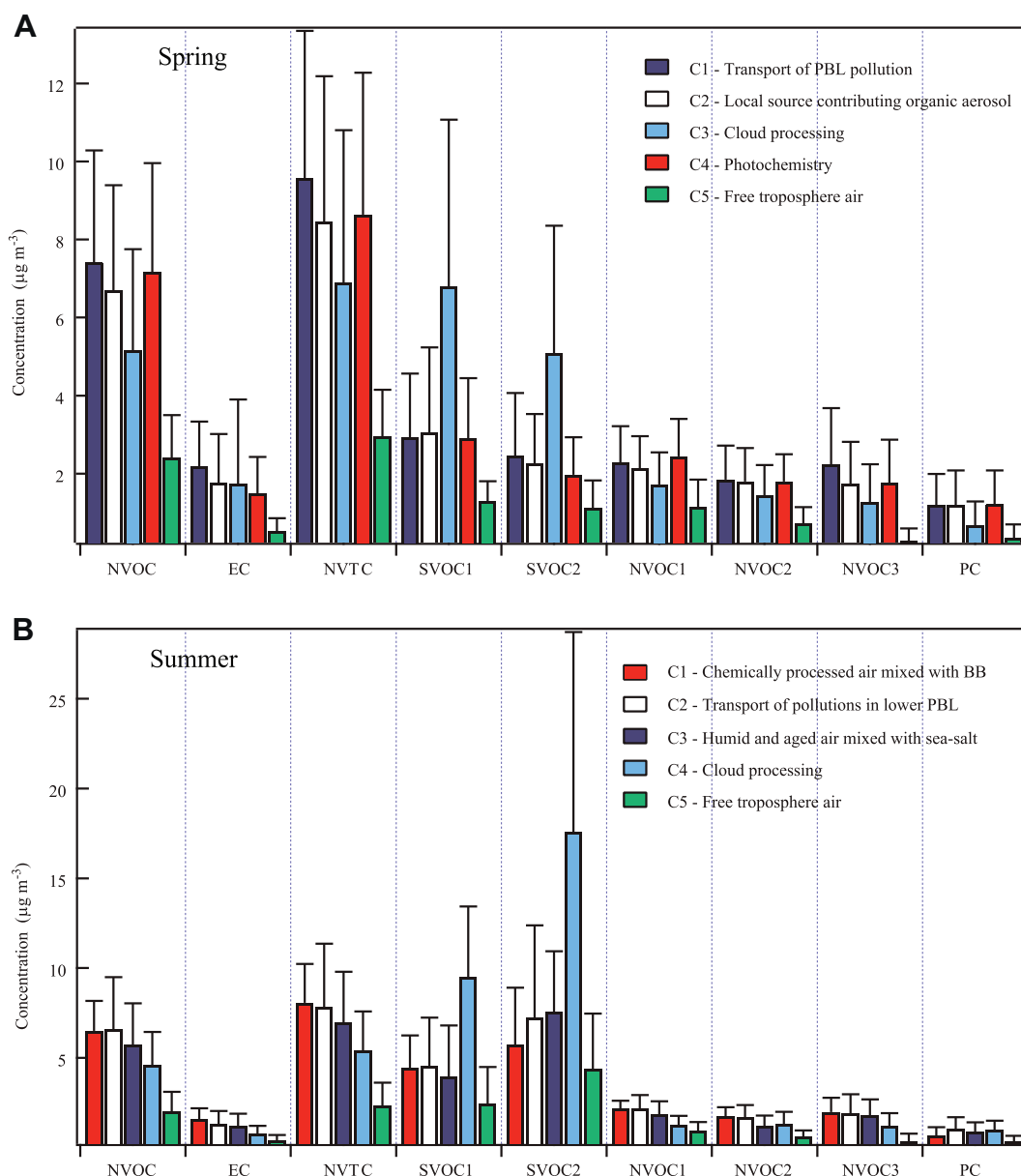


Fig. 9. The average concentrations of carbonaceous species for different groups dominated by identified sources in (A) spring and (B) summer based on HCA and PCA. The vertical bars represent the standard deviation of each species.

free troposphere air in both seasons, and are less than 30% of highest values among different groups. NVOC and EC in this group show similar concentrations in both seasons. Therefore, a general condition with $2.13 \pm 1.05 \mu\text{g m}^{-3}$ of NVOC and $0.43 \pm 0.29 \mu\text{g m}^{-3}$ of EC is suggested as the respective regional background over the North China Plain. However, SVOC varies with seasons, and thus a range of $2.40\text{--}6.80 \mu\text{g m}^{-3}$ is recommended for the background condition in this region.

4. Summary

A comprehensive study of non-volatile and semi-volatile carbonaceous aerosols was carried out at Mt. Tai in the North China Plain during spring and summer of 2007. NVOC, SVOC and EC showed higher concentrations than other background and mountain sites in the world. SVOC contributed to 51% and 72% of TOC concentration, indicating the importance of SVOC in total loading of organic carbon in the region. Different EC measurement methods presented good agreement, and the general relationship can be summarized as: Optical EC (660 nm) < Thermal EC \sim UVPM (370 nm) < BC (880 nm). However, because of the negative artifact from SVOC loss during sampling, the integrated filter measurement without denuder and backup absorbent significantly underestimated the TOC compared to semi-continuous measurement.

Source analysis based on PCA and HCA indicated that high carbonaceous concentrations were dominated by transport of PBL pollutions in both seasons, and clean air masses from the free troposphere provided the general background levels in the study area. The observed carbonaceous aerosols were more oxygenated and aged, and were often mixed with combined primary sources including biomass burning. Besides the sources in the North China Plains of China, the influence of emissions from Korea was observed at Mt. Tai, and was thought to partially contribute to the regional carbonaceous aerosol budget. Increased SVOC was associated with both cloud processing and photochemical production, and further discussion of SOA formation and cloud effect on SVOC will be presented in a future work.

Acknowledgments

This material is based upon work supported by the National Basic Research Project of China (973 Project No. 2005CB422203). The authors would like to thank Mr. Steven Poon, Dr. Wang Yan, Dr. Wang Jin, and Mr. Sun Tingli for the help on organizing the campaigns. The Mt. Tai Meteorological Observatory is gratefully acknowledged for its support of the field study and for providing the meteorological data. The authors acknowledge the NOAA Air Resources Laboratory for the provision of HYSPLIT model, and NASA/University of Maryland for providing the fire spot data. We thank Dr. Robert A. Cary, Dr. David Smith and Dr. Feng Bruce Dong for the technical support and discussions on the Sunset analyzer, Dr. Edward C. Mignot, Shandong University, for linguistic advice.

References

Bae, M.S., Schauer, J.J., DeMinter, J.T., Turner, J.R., Smith, D., Cary, R.A., 2004. Validation of a semi-continuous instrument for elemental carbon and organic carbon using a thermal-optical method. *Atmospheric Environment* 38, 2885–2893.

Bae, M.S., Hong, C.S., Kim, Y.J., Han, J.S., Moon, K.J., Kondo, Y., Komazaki, Y., Miyazaki, Y., 2007. Intercomparison of two different thermal-optical elemental carbons and optical black carbon during ABC-EAREX2005. *Atmospheric Environment* 41, 2791–2803.

Birch, M.E., Cary, R.A., 1996. Elemental carbon-based method for monitoring occupational exposures to particulate diesel exhaust. *Aerosol Science and Technology* 25, 221–241.

Cao, J.J., Lee, S.C., Chow, J.C., Watson, J.G., Ho, K.F., Zhang, R.J., Jin, Z.D., Shen, Z.X., Chen, G.C., Kang, Y.M., Zou, S.C., Zhang, L.Z., Qi, S.H., Dai, M.H., Cheng, Y., Hu, K.,

2007. Spatial and seasonal distributions of carbonaceous aerosols over China. *Journal of Geophysical Research-Atmospheres* 112. doi:10.1029/2006jd008205.

Cao, J.J., Xu, B.Q., He, J.Q., Liu, X.Q., Han, Y.M., Wang, G.H., Zhu, C.S., 2009. Concentrations, seasonal variations, and transport of carbonaceous aerosols at a remote Mountainous region in western China. *Atmospheric Environment* 43, 4444–4452.

Carrico, C.M., Bergin, M.H., Shrestha, A.B., Dibb, J.E., Gomes, L., Harris, J.M., 2003. The importance of carbon and mineral dust to seasonal aerosol properties in the Nepal Himalaya. *Atmospheric Environment* 37, 2811–2824.

Chan, T.W., Huang, L., Leaitch, W.R., Sharma, S., Brook, J.R., Slowik, J.G., Abbatt, J.P.D., Brickell, P.C., Liggio, J., Li, S.M., Moosmuller, H., 2010. Observations of OM/OC and specific attenuation coefficients (SAC) in ambient fine PM at a rural site in central Ontario, Canada. *Atmospheric Chemistry and Physics* 10, 2393–2411.

Cheng, Y., He, K.B., Duan, F.K., Zheng, M., Ma, Y.L., Tan, J.H., 2009. Positive sampling artifact of carbonaceous aerosols and its influence on the thermal–optical split of OC/EC. *Atmospheric Chemistry and Physics* 9, 7243–7256.

Cheng, Y., He, K.B., Duan, F.K., Zheng, M., Ma, Y.L., Tan, J.H., Du, Z.Y., 2010. Improved measurement of carbonaceous aerosol: evaluation of the sampling artifacts and inter-comparison of the thermal–optical analysis methods. *Atmospheric Chemistry and Physics* 10, 8533–8548.

Chow, J.C., Watson, J.G., Crow, D., Lowenthal, D.H., Merrifield, T., 2001. Comparison of IMPROVE and NIOSH carbon measurements. *Aerosol Science and Technology* 34, 23–34.

Chow, J.C., Chen, L.W.A., Watson, J.G., Lowenthal, D.H., Magliano, K.A., Turkiewicz, K., Lehrman, D.E., 2006. PM_{2.5} chemical composition and spatiotemporal variability during the California Regional PM₁₀/PM_{2.5} Air Quality Study (CRPAQS). *Journal of Geophysical Research-Atmospheres* 111. doi:10.1029/2005jd006457.

Dan, M., Zhuang, G.S., Li, X.X., Tao, H.R., Zhuang, Y.H., 2004. The characteristics of carbonaceous species and their sources in PM_{2.5} in Beijing. *Atmospheric Environment* 38, 3443–3452.

Fu, P.Q., Kawamura, K., Okuzawa, K., Aggarwal, S.G., Wang, G.H., Kanaya, Y., Wang, Z.F., 2008. Organic molecular compositions and temporal variations of summertime mountain aerosols over Mt. Tai, North China Plain. *Journal of Geophysical Research-Atmospheres* 113. doi:10.1029/2008jd009900.

Gao, J., Wang, T., Ding, A., Liu, C., 2005. Observational study of ozone and carbon monoxide at the summit of mount Tai (1534 m a.s.l.) in central-eastern China. *Atmospheric Environment* 39, 4779–4791.

Gelencser, A., May, B., Simpson, D., Sanchez-Ochoa, A., Kasper-Giebl, A., Puxbaum, H., Caseiro, A., Pio, C., Legrand, M., 2007. Source apportionment of PM_{2.5} organic aerosol over Europe: primary/secondary, natural/anthropogenic, and fossil/biogenic origin. *Journal of Geophysical Research-Atmospheres* 112. doi:10.1029/2006jd008094.

Grover, B.D., Eatough, N.L., Woolwine, W.R., Eatough, D.J., Cary, R.A., 2009. Modifications to the sunset laboratory carbon aerosol monitor for the simultaneous measurement of PM_{2.5} nonvolatile and semi-volatile carbonaceous material. *Journal of the Air & Waste Management Association* 59, 1007–1017.

Han, Y.M., Han, Z.W., Cao, J.J., Chow, J.C., Watson, J.G., An, Z.S., Liu, S.X., Zhang, R.J., 2008. Distribution and origin of carbonaceous aerosol over a rural high-mountain lake area, Northern China and its transport significance. *Atmospheric Environment* 42, 2405–2414.

Harrison, R.M., Yin, J.X., 2008. Sources and processes affecting carbonaceous aerosol in central England. *Atmospheric Environment* 42, 1413–1423.

Hennigan, C.J., Bergin, M.H., Weber, R.J., 2008. Correlations between water-soluble organic aerosol and water vapor: a synergistic effect from biogenic emissions? *Environmental Science & Technology* 42, 9079–9085.

Herckes, P., Chang, H., Lee, T., Collett, J.L., 2007. Air pollution processing by radiation fogs. *Water Air and Soil Pollution* 181, 65–75.

Hitzenberger, R., Berner, A., Giebl, H., Kromp, R., Larson, S.M., Rouc, A., Koch, A., Marischka, S., Puxbaum, H., 1999. Contribution of carbonaceous material to cloud condensation nuclei concentrations in European background (Mt. Sonnblick) and urban (Vienna) aerosols. *Atmospheric Environment* 23, 2647–2659.

Husain, L., Dutkiewicz, V.A., Khan, A., Ghauri, B.M., 2007. Characterization of carbonaceous aerosols in urban air. *Atmospheric Environment* 41, 6872–6883.

Jacobson, M.Z., 2001. Strong radiative heating due to the mixing state of black carbon in atmospheric aerosols. *Nature* 409, 695–697.

Jeong, C.H., Hopke, P.K., Kim, E., Lee, D.W., 2004. The comparison between thermal-optical transmittance elemental carbon and Aethalometer black carbon measured at multiple monitoring sites. *Atmospheric Environment* 38, 5193–5204.

Kanaya, Y., Komazaki, Y., Pochanart, P., Liu, Y., Akimoto, H., Gao, J., Wang, T., Wang, Z., 2008. Mass concentrations of black carbon measured by four instruments in the middle of Central East China in June 2006. *Atmospheric Chemistry and Physics* 8, 7637–7649.

Kondo, Y., Komazaki, Y., Miyazaki, Y., Moteki, N., Takegawa, N., Kodama, D., Deguchi, S., Nogami, M., Fukuda, M., Miyakawa, T., Morino, Y., Koike, M., Sakurai, H., Ehara, K., 2006. Temporal variations of elemental carbon in Tokyo. *Journal of Geophysical Research-Atmospheres* 111. doi:10.1029/2005jd006257.

Lim, H.J., Turpin, B.J., Edgerton, E., Hering, S.V., Allen, G., Maring, H., Solomon, P., 2003. Semicontinuous aerosol carbon measurements: comparison of Atlanta Supersite measurements. *Journal of Geophysical Research-Atmospheres* 108. doi:10.1029/2001jd001214.

Meng, Z.Y., Jiang, X.M., Yan, P., Lin, W.L., Zhang, H.D., Wang, Y., 2007. Characteristics and sources of PM_{2.5} and carbonaceous species during winter in Taiyuan, China. *Atmospheric Environment* 41, 6901–6908.

Menon, S., Hansen, J., Nazarenko, L., Luo, Y.F., 2002. Climate effects of black carbon aerosols in China and India. *Science* 297, 2250–2253.

- Morgan, W.T., Allan, J.D., Bower, K.N., Esselborn, M., Harris, B., Henzing, J.S., Highwood, E.J., Kiendler-Scharr, A., McMeeking, G.R., Mensah, A.A., Northway, M.J., Osborne, S., Williams, P.I., Krejci, R., Coe, H., 2010. Enhancement of the aerosol direct radiative effect by semi-volatile aerosol components: airborne measurements in North-Western Europe. *Atmospheric Chemistry and Physics* 10, 8151–8171.
- NASA/University of Maryland, 2002. MODIS hotspot/active fire detections. Data set. MODIS Rapid Response Project, NASA/GSFC (producer), University of Maryland, Fire Information for Resource Management System (distributors). Available on-line at: <http://maps.geog.umd.edu>.
- NIOSH, 1996. Element carbon (diesel particulate): method 5040. In: NIOSH Manual of Analytical Methods, fourth ed. (1st supplement). National Institute of Occupational Safety and Health, Cincinnati.
- Park, K., Chow, J.C., Watson, J.G., Trimble, D.L., Doraiswamy, P., Arnott, W.P., Stroud, K.R., Bowers, K., Bode, R., Petzold, A., Hansen, A.D.A., 2006. Comparison of continuous and filter-based carbon measurements at the Fresno Supersite. *Journal of the Air & Waste Management Association* 56, 474–491.
- Plaza, J., Gomez-Moreno, F.J., Nunez, L., Pujadas, M., Artinano, B., 2006. Estimation of secondary organic aerosol formation from semicontinuous OC-EC measurements in a Madrid suburban area. *Atmospheric Environment* 40, 1134–1147.
- Puxbaum, H., Rendl, J., Allabashi, R., Otter, L., Scholes, M.C., 2000. Mass balance of the atmospheric aerosol in a South African subtropical savanna (Nylsvley, May 1997). *Journal of Geophysical Research-Atmospheres* 105, 20697–20706.
- Ram, K., Sarin, M.M., Hegde, P., 2008. Atmospheric abundances of primary and secondary carbonaceous species at two high-altitude sites in India: Sources and temporal variability. *Atmospheric Environment* 42, 6785–6796.
- Ren, Y., Ding, A., Wang, T., Shen, X., Guo, J., Zhang, J., Wang, Y., Xu, P., Wang, X., Gao, J., Collett Jr., J.L., 2009. Measurement of gas-phase total peroxides at the summit of Mount Tai in China. *Atmospheric Environment* 43, 1702–1711.
- Rengarajan, R., Sarin, M.M., Sudheer, A.K., 2007. Carbonaceous and inorganic species in atmospheric aerosols during wintertime over urban and high-altitude sites in North India. *Journal of Geophysical Research-Atmospheres* 112. doi:10.1029/2006jd008150.
- Saarikoski, S., Timonen, H., Saarnio, K., Aurela, M., Jarvi, L., Keronen, P., Kerminen, V.M., Hillamo, R., 2008. Sources of organic carbon in fine particulate matter in northern European urban air. *Atmospheric Chemistry and Physics* 8, 6281–6295.
- Seinfeld, J.H., Pandis, S.N., 1998. *Atmospheric Chemistry and Physics: From Air Pollution to Climate Change*. John Wiley, New York.
- Sun, J.M., Ariya, P.A., 2006. Atmospheric organic and bio-aerosols as cloud condensation nuclei (CCN): a review. *Atmospheric Environment* 40, 795–820.
- Watson, J.G., Chow, J.C., Houck, J.E., 2001. PM_{2.5} chemical source profiles for vehicle exhaust, vegetative burning, geological material, and coal burning in North-western Colorado during 1995. *Chemosphere* 43, 1141–1151.
- Yttri, K.E., Aas, W., Bjerke, A., Cape, J.N., Cavalli, F., Ceburnis, D., Dye, C., Emblico, L., Facchini, M.C., Forster, C., Hanssen, J.E., Hansson, H.C., Jennings, S.G., Maenhaut, W., Putaud, J.P., Torseth, K., 2007. Elemental and organic carbon in PM₁₀: a one year measurement campaign within the European Monitoring and Evaluation Programme EMEP. *Atmospheric Chemistry and Physics* 7, 5711–5725.
- Zhang, Q., Streets, D.G., Carmichael, G.R., He, K.B., Huo, H., Kannari, A., Klimont, Z., Park, I.S., Reddy, S., Fu, J.S., Chen, D., Duan, L., Lei, Y., Wang, L.T., Yao, Z.L., 2009. Asian emissions in 2006 for the NASA INTEX-B mission. *Atmospheric Chemistry and Physics* 9, 5131–5153.
- Zhang, X.Y., Wang, Y.Q., Zhang, X.C., Guo, W., Gong, S.L., 2008. Carbonaceous aerosol composition over various regions of China during 2006. *Journal of Geophysical Research-Atmospheres* 113. doi:10.1029/2007jd009525.
- Zhou, X., Gao, J., Wang, T., Wu, W., Wang, W., 2009. Measurement of black carbon aerosols near two Chinese megacities and the implications for improving emission inventories. *Atmospheric Environment* 43, 3918–3924.
- Zhou, Y., Wang, T., Gao, X., Xue, L., Wang, X., Wang, Z., Gao, J., Zhang, Q., Wang, W., 2010. Continuous observations of water-soluble ions in PM_{2.5} at Mount Tai (1534 m a.s.l.) in central-eastern China. *Journal of Atmospheric Chemistry* 64, 107–127.